# Optimizing light delivery in scanning photoacoustic imaging for prostate*

**PENG Dong-qing** (彭东青)[1], **LIU Zhi-gao** (刘志高)[1], **XU Hui-zhen** (徐惠真)[1], **ZHU Li-li** (朱莉莉)[2], **and LI Hui** (李晖)[2]**

*1. School of Science, Jimei University, Xiamen 361021, China*

*2. Key Laboratory of Optoelectronic Science and Technology for Medicine (Ministry of Education of China), Fujian Provincial Key Laboratory of Photonic Technology, College of Photonic and Electronic Engineering, Fujian Normal University, Fuzhou 350007, China*

(Received 7 May 2020; Revised 17 July 2020)



The purpose of this study was to optimize the light delivery method in a prostate photoacoustic imaging system. A three dimensional (3D) optical model of the human prostate was developed, and the optical energy distribution in the prostate was estimated via three-dimensional Monte Carlo simulation. Then, the feasibility of prostate photoacoustic imaging (PAI) using two endoscopic light delivery methods was studied. Photoacoustic pressure generation and the corresponding photoacoustic images had been obtained and the comparisons were made between each other. Also, the results of cylinder diffusing light source with different lengths were compared. After that, phantom experiment was carried out to validate the simulation results. Our results would be significant in the optimizing photoacoustic imaging system for an accurate diagnosis of prostate cancer.

**Document code:** A **Article ID:** 1673-1905(2021)01-0053-6

**DOI** https://doi.org/10.1007/s11801-021-0077-7

In recent years, prostate cancer has been a serious health concern around the world, especially in the United States[1]. As a new imaging modality for various biomedical applications which combined contrast capability of optical imaging with the resolution of ultrasound imaging, photoacoustic imaging (PAI) has recently emerged as a promising imaging technique for imaging prostate lesions[2-5]. At present, transrectal light illumination (TRLI) and transurethral light illumination (TULI) had both been used as light irradiation model in the PAI studies of prostate. Yaseen et al[6] and Valluru et al[7] had performed photoacoustic imaging of prostate cancer by TRLI, although it was minimally invasive，however, this approach was limited by poor light penetration through the rectal wall. Recently, handheld photoacoustic probe was built to improve imaging sensitivity by integrating optical components with a transrectal transducer array[8,9]. At the same time, PAI through TULI was also carried out in phantom experiment[10], to monitor the seed in the radiotherapy of prostate cancer[11,12], and PAI probe with transurethral illumination was recently developed in order to gain a whole-prostate imaging[13,14]. Therefore, there was still some critical issues to be considered in the PAI for prostate cancer detection, such as an optimal light delivery to prostate with a sufficient penetrating depth. Technical optimization of light delivery modality in the PAI instrumentation of prostate would improve accuracy and sensitivity of imaging system, and would propel its translation toward clinical application.

In order to optimize the laser delivery in the PAI system for prostate, in the letter, a three dimensional (3D) prostate optical model was firstly established according to the structure of human prostate. Optical energy deposition characteristics were compared between TULI and TRLI with Monte Carlo simulation method, and photoacoustic pressure was calculated based on the velocity potential[15] considering transrectal pressure sensing since of its convenience for clinical practice. Meanwhile, comparison of optical energy deposition between different length of cylindrical diffuser used for TULI was studied. In addition, imaging in the agar phantom and pig pork was carried out.

The histological structure of the prostate was shown in Fig.1(a). The prostate was a small muscular gland beneath urinary bladder, which surrounds the urethra as it exited the bladder. And rectum was next to the prostate. 3D matrix was used to simulate the structure of human prostate tissue and anatomical models. The key of using 3D matrix to simulate human tissue was the size division of each voxel. The 3D Cartesian matrix of voxels was

* This work has been supported by the National Natural Science Foundation of China (No.61675043), the Natural Science Foundation of Fujian Province (No.2018J01416), the Key Laboratory of OptoElectronic Science and Technology for Medicine of Ministry of Education (No.JYG1808), and the National Fund Cultivation Plan of Jimei University (No.ZP2020059).

** E-mail: hli@fjnu.edu.cn

established through programming by MATLAB software, each voxel was assigned a tissue type. And each tissue type has a unique set of optical properties (absorption coefficient $\mu_a$, scattering coefficient $\mu_s$, anisotropy of scattering $g$). As shown in Fig.1(b), the proposed 3D model consisted of an ellipsoid prostate with a size of 30 mm×30 mm×40 mm, a cylindrical-shaped urethra with an external diameter of 4 mm and an inner diameter of 3 mm, a rectum with a 1-mm-thick rectal wall and internal diameter of 20 mm. Muscle with thicknesses of 4.5 mm were covering the rectal wall. The background was filled with adipose tissue.

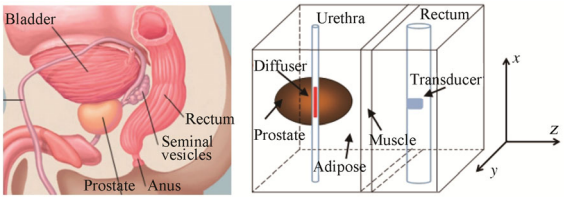


(a) (b)

**Fig.1 (a) Histological structure and (b) 3D model of the prostate**

Monte Carlo simulation was adopted to understand the light propagation within the proposed 3D model at a specific wavelength of $\lambda$=1 000 nm which can produce a high contrast in laser fluence for the prostate and its neighboring tissues. For the chosen wavelength, the optical properties for prostate and surrounding tissues were summarized in Tab.1[16-19]. Approximately 1.6 million photons were randomly generated to guarantee accuracy in calculations.

**Tab.1 Optical properties of prostate, tumor and the neighboring tissues at $\lambda$=1 000 nm**

| Tissue | $\mu_a$ (1/cm) | $\mu_s$ (1/cm) | $g$ |
|---|---|---|---|
| Air | 0.001 | 10 | 1.0 |
| Rectal wall | 3.3 | 230.8 | 0.93 |
| Muscle | 0.51 | 81.9 | 0.93 |
| Urethra wall | 0.24 | 43.3 | 0.65 |
| Prostate | 0.4 | 34 | 0.86 |
| Tumor | 20.9 | 330 | 0.951 |
| Adipose | 3.0 | 37 | 0.91 |

The method of calculating the stress wave that reaches the detector was based on the velocity potential $\phi(t)$, which was related to the spatial distribution of energy deposition $W$. At each time point after the impulse of energy deposition, a spherical shell of deposited energy $W_{shell}$, with a radius $r=C_s t$ centered on the detector would have launched a stress wave that arrived at the detector at time $t$. And the value $\phi(t)$ was positive and can be calculated by[15]

$$-\phi(t)=\frac{\beta}{4\pi\rho C_p}\frac{1}{\mathrm{d}t}\int_{r-\mathrm{d}r/2}^{r+\mathrm{d}r/2}\frac{W_{shell}}{r}4\pi r^2\mathrm{d}r\,, \tag{1}$$

where $r$ was the distance from shell to detector at time $t$, which was the time of stress wave arrival at detector, d$t$ was time step of integration, d$t$=d$z$/$C_s$, $C_s$ was speed of sound in tissue and was 1 500 m/s, $\beta$ was thermal expansivity, and $\beta$=2.57×10$^{-4}$ °C$^{-1}$, such that $\Gamma$≈0.138 at tissue temperature. $\rho$ was density, $\rho$≈1 000 kg/m$^3$, $C_p$ was specific heat, $C_p$=4 180 J/(kg.°C), $W_{shell}$ was the average energy deposition in shell, which was calculated discretely using the Monte Carlo array $W$.

Therefore, the magnitude of the velocity potential $\phi(t)$ arriving at time $t$ was proportional to the energy deposited in $W_{shell}$, at a distance $r$ from the detector. The photoacoustic pressure $P$ was related to $\phi(t)$:

$$P=-\rho\frac{\mathrm{d}\phi}{\mathrm{d}t}\,. \tag{2}$$

In the letter, the distribution image of light energy deposition $W$ was obtained by 3D Monte Carlo simulation, and the photoacoustic (PA) pressure received by focusing transducer placed in the rectum was calculated according to the method above, Once the time-resolved PA pressure was obtained by each position of the detector, a Hilbert transform algorithm was used to reconstruct a two-dimensional (2D) PAI of prostate tissue.

Fig.2 shows the prostate optical model generated by MATLAB software, using TULI and TRLI. An isotropic cylindrical diffused light source (CDLS) with a length of 20 mm was used. Two spherical tumors with a radius of 2 mm were embedded at upper and lower side 10 mm from the center of urethra, as shown in Fig.2. Fig.3 shows 2D absorption maps by 3D Monte Carlo simulation under these two illumination methods. It was numerically confirmed that there was a full light absorption within the prostate tissue through TULI, as shown in Fig.3(a). It should be emphasized that the tumors have a higher absorption than the neighboring normal prostate tissue due to its relatively larger absorption coefficient, and noting that, there was a symmetrical light absorption property around the light source. The optical energy absorption of tumor at upper side of the light source was almost the same to that of lower side. The penetrating light that reached the tumor elicited strong energy deposition in the superficial layers of the tumor. On the other hand, in the TRLI, lots of the light absorption happened outside the prostate, there was absorption only in the vicinity of prostate since of the attenuation of surrounding tissue. Most of the incident photons was absorbed by rectal wall, muscle and fat layers, as shown in Fig.3(b). And, the total absorption power in the tumor in trans-urethral case was much larger than the value of trans-rectal case. Thus, we can image the prostate tumor only in the vicinity of the rectal wall layer. Simulation indicated that laser illumination from urethra would allow the prostate tissue to obtain a more efficient light absorption than TRLI. Similar findings were also given by EI-Gohary et al[20], Tang et al[21] and Peng et al[22]. Therefore, TULI method has the possibility of imaging the whole volume of the prostate, and a larger detection

depth in the PA probe was feasible since the photoacoustic probe was loaded at a rectal wall.

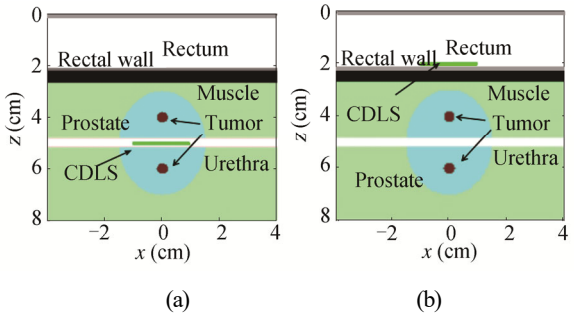


**Fig.2 *zx*-plane of prostate optical model generated by MATLAB using (a)TULI and (b) TRLI**

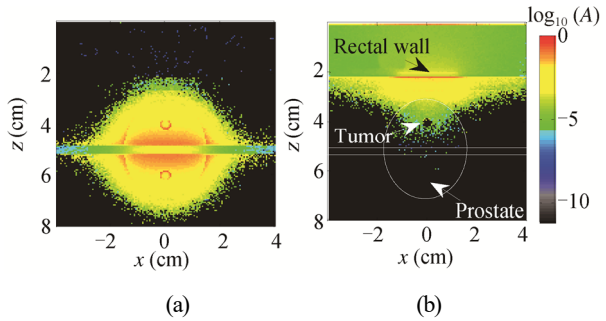


**Fig.3 Optical energy deposition characteristics produced by CDLS through (a) TULI and (b) TRLI**

Next, we investigated the PA signal generation and image reconstruction with these two illumination methods while a focusing transducer was used for transrectal PA pressure detection. The time-resolved PA pressure was calculated according to the velocity potential. Hilbert coefficient of PA pressure along $x$=0 through TULI and TRLI was demonstrated in Fig.4. As shown in Fig.4(a), it was observed that, using TULI, there were several peaks in the PA pressure profile, which were caused by dramatic change of PA pressure amplitude at the urethra and tumor boundaries since of the sudden variation of optical energy deposition at these boundaries. From these peaks, location and size of tumor can be detected easily. However, only the boundaries of rectal wall could be seen using TRLI, as shown in Fig.4(b) .

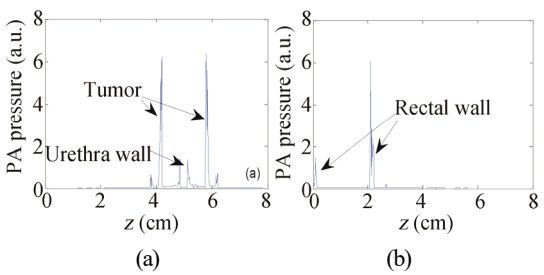


**Fig.4 Hilbert coefficient of PA pressure along $x$=0 through (a) TULI and (b) TRLI**

The 2D PA image could be obtained by combining the time resolved PA pressure obtained by each position of the detector. Fig.5 shows the PA image reconstructed for the two light delivery methods. Among them, PAI using TULI exhibited the higher PA signal amplitude of prostate tumor, and the images of these two tumors at anterior and posterior of the prostate could be seen easily since that there was a high signal-to-noise ratio. It was attributed to the fact that a greater absorption in the prostate tumor can be achieved by TULI. Therefore, the imaging depth could be improved since transrectal photoacoustic detector was used. For the case of TRLI, delivered photons at the tumor were very few due to a high absorption of rectal wall, muscle layers and adipose tissue. Thus, the amplitude of the generated PA pressure in the tumor was insignificant and tumors were indistinguishable.

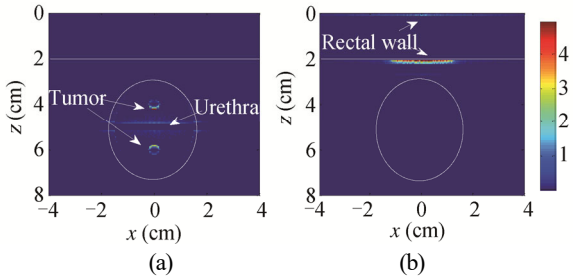


**Fig. 5 Photoacoustic images produced by CDLS: (a) TULI; (b) TRLI**

In order to deliver an optical energy more efficiently to prostate tumor, in this section, we showed a comparison of optical energy deposition between different length of cylindrical diffuser used for TULI in the 3D prostate model without tumor embedded. Six different lengths of the cylindrical diffuser were considered in the light illumination. Fig.6 shows the optical energy deposition results. Comparing Fig.6(a)—(f), it can be found that there were a gradual increase in the lateral range of uniform absorbed light energy distribution and illumination area within the prostate model as the length increased. While its value of absorbed light energy near the urethra decreased as the length increased which hinted light energy was allowed to increase to further imaging depth never mind destroying the urethral wall. Since that the prostate size increases and varies in a wide range with advancing age, an optimal length of diffusing light should be adopted to match the dimension along the urethra to illuminate enough volume of prostate, while carrying out the PAI for prostate tissue by TULI.

PAI experiment had been carried out, in which endoscopic light illumination simulating TULI for photoacoustic signal generation was used. A mechanical scanning photoacoustic imaging system was utilized, as shown in Fig.7. A Q-switched Nd:YAG laser (Surelite I-10, Continuum, West Newton, MA, USA) was used for photoacoustic wave generation with a wavelength of 532 nm, a repetition frequency of 10 Hz, a pulse width of 6 ns, and output energy of ~4 mJ. The laser beam was

divided into two beams using a beam splitter (BS). One beam was received by a positive intrinsic-negative photodiode (PIN) (ET-2030, Electro-Optics Technology,Inc) and displayed on an oscilloscope (TDS3054C, Tektronix, Johnston, OH, USA) for calibration, while the other was coupled into a cylindrical diffusing fiber which would be inserted to the phantom to generate the photoacoustic signal. The optical fiber was a customized product from Wuhan Baiheng Medical Technology Corp. Ltd, with transmission band of 490—800 nm and SMA905 standard interface. The diffuser distal end was 20 mm in length and 1.5 mm in diameter. An immersion long-zone focus transducer with central frequency of 3.5 MHz, focus length of 60 mm, 30.3 mm extended focal zone (V381, Parametrics NDT, USA) was mounting on an electronic translation machine (TSA200-B, Zolix) driven by a step motor (SC300-2B, Zolix, Beijing, China) to receive acoustic signal. Tissue phantom which was internal illuminated by diffusing fiber was located below a water tank with a 50 mm diameter plastic wrap at the center of the bottom. The depth-resolved photoacoustic signals from the sample was collected by the transducer immersed in the water tank and was then transferred to an ultrasonic receiver (5800PR, Parametric-NDT, Hamburg, Germany) for amplitude filtering and amplification. Finally, the signals were sent to the digital oscilloscope (TDS3054C, Tektronix, Johnston, OH, USA), and were averaged 64 times. Through moving the transducer using computer controlled step-motors at an interval of 0.2 mm, 2D PAI can be obtained.

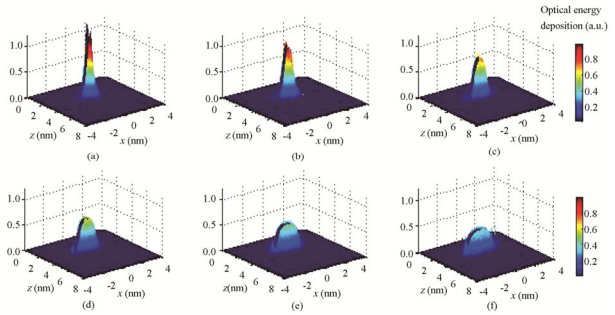


**Fig.6 Optical energy deposition when the length of CDLS increases from 4 mm to 24 mm as a step of 4 mm: (a) 4 mm; (b) 8 mm; (c) 12 mm; (d) 16 mm; (e) 20 mm; (f) 24 mm**

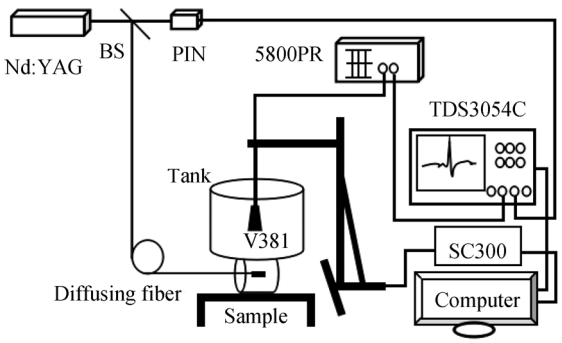


**Fig.7 PAI experimental setup**

A cuboid agar phantom was used for the experiments, which was made of agar gel with intralipid as scatterers and ink as absorbers. The homogeneous scattering phantom contained 2 g agar powder, 2 mL intralipid-20% solution (SinoSwed Pharmaceutical Corp. Ltd), and 100 ml distilled water. Endoscopic light delivery was utilized by cylindrical diffuser fiber which was inserted in a hole with diameter of 1.5 mm reserved in the middle of the phantom simulating urethra, as shown in Fig.8(a). And in Fig.8(b), four carbon absorbers were embedded in the cuboid phantom around the cylindrical diffuser fiber. The reconstructed 2D photoacoustic image was shown in Fig.8(c). We can find that the 2D photoacoustic image was well consistent with the actual absorber, which reflected well the position and distance of the carbon absorber. and the strong signal pointed by arrow fiber was excited by the cylindrical diffusing fiber itself. Noting that these four carbons around the diffuser fiber were all clear, irrespective of their positions. Result showed transurethral method has the possibility of imaging the whole volume of the phantom.

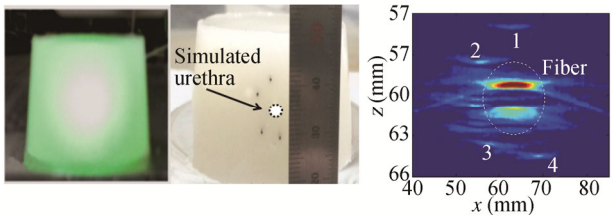


**Fig.8 (a) Endoscopic light delivery for phantom; (b) Experimental phantom; (c) The reconstructed 2D photoacoustic image**

In order to show that the constructed photoacoustic imaging system has the ability of imaging the real biological tissue, the scanning imaging of the pork tissue embedded with blood injection rubber tube was further carried out. The blood injected into the rubber tube was not treated with anticoagulant. The blood clot was imaged in the experiment. Fig.9(a) shows three transparent blood injection tubes with an inner diameter of 1mm.The experimental pork sample shown in Fig.9(b) was about 30 mm thick. The cylindrical diffuser fiber was inserted in position *O*, two simulated blood vessels were embedded at positions *A*, *B*, respectively, at a distance of about 5 mm between the upper of the optical fiber, and another simulated blood vessel was embedded at positions *C* under the fiber at a distance of about 7 mm. Fig.9(c) shows the photo of the sample by endoscopic light illumination. As shown in Fig.9(d), the results of photoacoustic scanning showed that the images of *A*, *B* and *C* vessels were all clear and distinguishable, and their relative positions were consistent with the actual model. The above real biological sample experiments validated further that the endoscopic light delivery was helpful for efficient light absorption and imaging the entire volume of tissue.

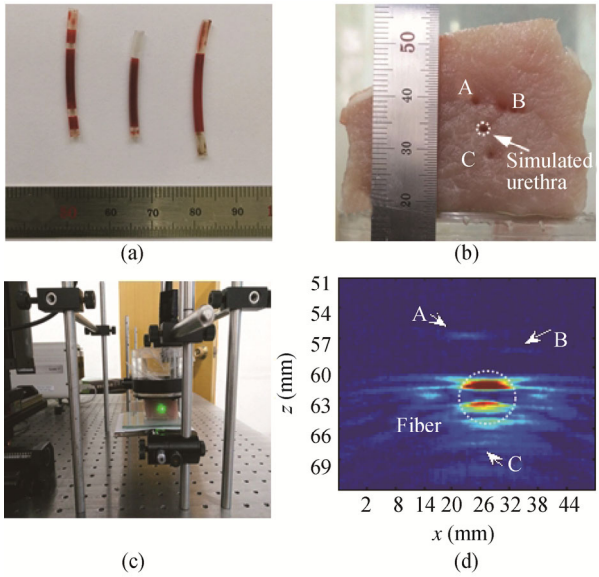


**Fig.9 (a) Simulated blood vessel; (b) Photo of experiment sample; (c) Endoscopic light delivery for pork tissue; (d) 2D photoacoustic imaging result**

As a usual light illumination model in the PAI studies, TRLI was difficult to obtain an accurate reconstructed photoacoustic image. It was suffering from a great of light absorption attenuation due to the surrounding scattering tissue. Some particular methods were required to be considered in the photoacoustic imaging technique for prostate, such as a light delivery to prostate with a sufficient penetrating depth and a minimal invasiveness. In order to optimize the laser delivery in the photoacoustic imaging system for prostate, in this letter, a 3D prostate optical model was firstly established according to the structure of human prostate. The optical energy deposition was calculated by 3D Monte Carlo simulation. And the calculating of stress wave was based on the velocity potential. The effectivity of prostate PAI using TULI and TRLI were studied. In addition, the photoacoustic imaging experiment was carried out in agar model and pork tissue. Results showed that TULI method has the ability to cover the whole volume of the prostate providing enough detectable acoustic pressure, while TRLI could only image a prostate tumor in the vicinity of the rectal wall. Urologists preferred a transrectal transducer because it was convenient for clinical practice. Therefore, a transrectal ultrasound transducer was widely used in urology. Although it was much easier to integrate a laser source to the transrectal ultrasound transducer, our simulation result showed that, by use of TRLI, little optical energy could penetrate to the prostate tissue. Most of the incident photons was absorbed by rectal wall, muscle and fat layers, which leading to a difficulty for illuminating the whole volume of the prostate, thus degrading the imaging quality when the tumor was far away from the rectum. Because of the symmetrical light emitting characteristic of CDLS and a relatively better lateral uniformity of light absorption around the light source through TULI, the light absorption of tumor at the upper side of the light source was almost the same to that of lower side. Therefore, the imaging depth and lateral imaging range could be improved. In addition, an optimal length of diffusing light should be adopted to match the dimension along the urethra to illuminate enough volume of prostate, while carrying out the PAI for prostate tissue by TULI. In conclusion, the combination of transurethral laser and transrectal detector should be presently the optimized configuration in clinical practice for prostate PAI. The conclusions help to optimize the light delivery method in a prostate PAI system. In the near future, the PAI system would be applicable to prostate tissue in vivo and animal models and can be reported in a separate paper.

## References

[1] R L Siegel, K D Miller and A Jemal, Cancer Statistics, CA: A Cancer Journal for Clinicians **68**, 7 (2018).

[2] X Wang, W W Roberts, P L Carson, D P Wood and J B Fowlkes, Biomedical Optics Express **1**, 1117 (2010).

[3] S R Kothapalli, GA Sonn, J W Choe, A Nikoozadeh, A Bhuyan, K K Park, P Cristman, R Fan, A Moini, B C Lee, J Wu, T E Carver, D Trivedi, L Shiiba, I Steinberg, D M Huland, M F Rasmussen, J C Liao, J D Brooks, P T Khuri-Yakub and S S Gambhir,, Science Translational Medicine **11**, eaav2169 (2019).

[4] V S Dogra, B K Chinni, K S Valluru, J V Joseph, A Ghazi, J L Yao, K Evans, E M Messing and N A Rao, Journal of Clinical Imaging Scienc **3**, 41 (2013).

[5] A Agarwal, S W Huang, M O Donnell, K C Day, M Day, N Kotov and S Ashkenazi, Journal of Applied Physics **102**, 064701 (2007).

[6] M A Yaseen, S A Ermilov, H Brecht, R Su, A Conjusteau, M Fronheiser, B A Bell, M Motamedi and A A Oraevsky, Journal of Biomedical Optics **15**, 21310 (2010).

[7] K Valluru, B Chinni, S Bhatt, V Dogra, N A Rao and D Akata, Probe Design for Photoacoustic Imaging of Prostate, IEEE International Conference on Imaging Systems and Techniques, 121 (2010).

[8] A. Horiguchi, M. Shinchi, A. Nakamura, T. Wada, K. Ito, T. Asano, H. Shinmoto, H. Tsuda and M. Ishihara, Urology **108**, 212 (2017).

[9] C B Liu, M Y Xing, B Cong, C Qiu, D He, C Z Wang, Y Xiao, T H Yin, M Shao, W B Qiu, T Ma, X J Gong, X Chen, H R Zheng, R Q Zheng and L Song, Biomedical Optics Express **10**, 1707 (2019).

[10] W M Xie, L Li, Z F Li and H Li, Photoacoustic Imaging of Prostate Cancer using Cylinder Diffuse Radiation, Proceedings of SPIE, 85532V (2012).

[11] M A L Bell, N P Kuo, D Y Song, J U Kang and E M Boctor, Journal of Biomedical Optics **19**, 126011 (2014).

[12] M A L Bell, X Y Guo, D Y Song and E M Boctor, Journal of Biomedical Optics **20**, 036002 (2015).

[13] M Ai, J I Youn, S E Salcudean, R Rohling, P

Abolmaesumi and S Tang, Biomedical Optical Express **10**, 2588 (2019).

[14] B Bungart, Y C Cao, T Yang-Tran, S Gorsky, L Lan, D Roblyer, M O Koch, L Cheng, T Masterson, J X Cheng, Biomedical Optics Express **10**, 1405 (2019).

[15] S L Jacques, Photoacoustics **2**, 137 (2014).

[16] T Vo-Dinh, Biomedical Photonics Handbook, BocaRaton: CRC Press, 2003.

[17] D Boas, C Pitris and N Ramanujam. Handbook of Biomedical Optics, Boca Raton: CRC Press, 2011.

[18] P Agrba, M Kirillin, A Abelevich and V Kamensky, Mechanical Compression for Biotissue Image Enhancement in Optical Coherence Tomography, Proceedings of SPIE, 754703 (2010).

[19] T Svensson, S Andersson-Engels, M Einarsdóttír and K Svanberg, Journal of Biomedical Optics **2**, 014022 (2007).

[20] S H El-Gohary, M K Metwally, S Eom, S H Jeon, K M Byun and T S Kim, Biomedical Engineering Letters **4**, 250 (2014).

[21] S Tang, J Chen, P Samant, K Stratton and L Xiang, IEEE Transactions on Medical Imaging **35**, 1780 (2016).

[22] D Q Peng, Y Y Peng, J Guo and H Li, Laser Illumination Modality of Photoacoustic Imaging Technique for Prostate Cancer, Journal of Physics: Conference Series **679**, 012026 (2016).